

Geometry-constrained Car Recognition Using a 3D Perspective Network

Rui Zeng[†], Zongyuan Ge^{‡*}, Simon Denman[†], Sridha Sridharan[†], Clinton Fookes[†]

[†]Queensland University of Technology
Brisbane, Australia

{r5.zeng, s.denman, s.sridha, c.fookes}@qut.edu.au

[‡]Monash University
Melbourne, Australia

{zongyuan.ge}@monash.edu

Abstract

We present a novel learning framework for vehicle recognition from a single RGB image. Unlike existing methods which only use attention mechanisms to locate 2D discriminative information, our unified framework learns a joint representation of the 2D global texture and 3D-bounding-box in a mutually correlated and reinforced way. These two kinds of feature representation are combined by a novel fusion network, which predicts the vehicle's category. The 2D global feature is extracted using an off-the-shelf detection network, where the estimated 2D bounding box assists in finding the region of interest (RoI). With the assistance of the RoI, the 3D bounding box and its corresponding features are generated in a geometrically correct way using a novel 3D perspective Network (3DPN). The 3DPN consists of a convolutional neural network (CNN), a vanishing point loss, and RoI perspective layers. The CNN regresses the 3D bounding box under the guidance of the proposed vanishing point loss, which provides a perspective geometry constraint. Thanks to the proposed RoI perspective layer, the variation caused by viewpoint changes is corrected via the estimated geometry, enhancing the feature representation. We present qualitative and quantitative results for our approach on the vehicle classification and verification tasks in the BoxCars dataset. The results demonstrate that, by learning how to extract features from the 3D bounding box, we can achieve comparable or superior performance to methods that only use 2D information.

1. Introduction

Traffic surveillance systems are an important part of intelligent transportation, which has already been deployed widely all over the world for regulating and monitoring traffic in cities. A holy grail for traffic surveillance is the ability to automatically recognize and identify vehicles from visual information alone. Vehicle recognition enables automated car

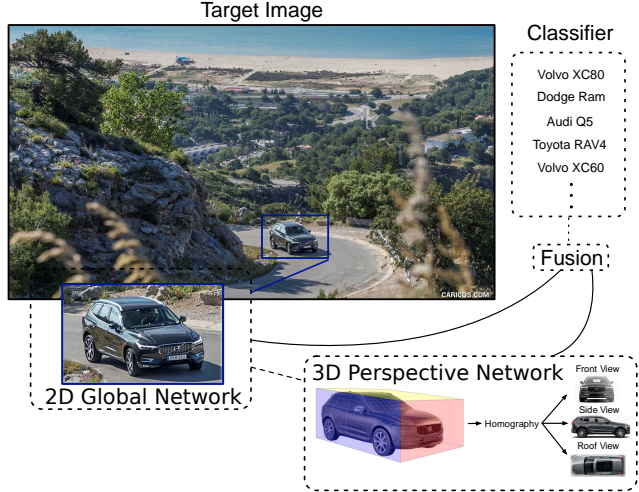


Figure 1: Consider the image of the car shown above. Even though the vehicle is shown on a flat 2D image, our model can estimate and leverage knowledge from 2D appearance as well as the rigid 3D bounding box of the vehicle to produce a viewpoint-normalized representation, which is able to improve vehicle recognition performance.

model analysis, which is helpful for innumerable purposes including regulation, description, and indexing vehicles.

One key idea shared by recent vehicle recognition algorithms is to use an ensemble of local features extracted from discriminative parts of the vehicle, which can be located using either part annotations or attention mechanisms. These approaches, given part annotations, [9, 14] learn the corresponding part detectors and then assemble these to obtain a uniform representation of the vehicle, which is used for category classification. To overcome the need for part annotations, recent advances [13, 15, 22, 30, 33] make use of attention mechanisms to identify salient spatial regions automatically. Despite these part-aware methods successfully leveraging spatial information, they are still ‘flat’, i.e., built on independent and 2D views.

3D-aware methods have been shown to be promising

* indicates the corresponding authorship

alternatives to part-aware approaches. For instance, [16, 21] exploit the fact that aligning a 3D CAD model or shape to 2D images significantly eliminates the variation caused by viewpoint changes, which is shown as the main obstacle for vehicle categorization. However, these methods have limited generality as they require 3D CAD models for vehicles.

To address these issues, we instead propose to directly use the 3D bounding box of the vehicle to normalize viewpoint variation. Our work is summarized in Figure 1. It combines the benefits of a 3D bounding box representation with a 2D appearance-based depiction of a vehicle. Our proposed method has three components: the Global Network (GN), the 3D Perspective Network (3DPN), and the Feature Fusion Network (FFN). The GN detects and extracts relevant global appearance features of vehicles from input RGB images. The 3DPN predicts the 3D bounding box under the geometric constraints of the vanishing points using the proposed vanishing point loss. With the assistance of the predicted 3D bounding box, the 3DPN further generates a viewpoint-aligned feature representation using the proposed ROI perspective pooling layer to extract 3D data in a geometrically correct manner. Finally, the features generated from the GN and the 3DPN are merged in the FFN and then used for vehicle recognition. Our contributions can be summarized as follows:

- A unified network architecture for vehicle recognition which takes full advantage of the 2D and 3D representations is presented. To our best knowledge, our method is the first work which extracts a meaningful feature representation from the 3D bounding box to enhance vehicle recognition.
- A 3D bounding box predictor, i.e. 3DPN, is proposed for vehicle recognition to use 3D information in a meaningful and correct manner, without the challenge of requiring a 3D CAD model.
- We propose a new parameterized CNN pooling layer termed ROI Perspective pooling, which grants the CNN the adaptive transformation modeling capability to normalize vehicle viewpoints in the feature space given the 3D bounding box.
- We introduce a geometrically interpretable loss (vanishing point loss) to elegantly enforce the consistency of the predicted 3D bounding box to improve regression accuracy.

We evaluate our proposed method on the vehicle classification and verification tasks in the BoxCars benchmark and show that without using 3D annotations, we achieve better results than the state-of-the-art methods that only use 2D information.

2. Related Work

We review the previous works on vehicle recognition, cuboid detection, and ROI pooling, which are related to our ap-

proach.

Vehicle classification: Since our model uses only a single image to recognize vehicles, methods which use extra information, such as 3D CAD models, are not reviewed. 2D vehicle recognition can be classified into two categories: part-annotation (PA) and attention-mechanism (AM) methods. While PA methods [9, 14, 25] are able to achieve high performance by extracting local feature representation from detected vehicle parts, they are reliant on part annotations. The labor intensive annotation is usually not possible during inference when applying such methods to a real scene. [9] detects each discriminative part of a vehicle and then generates a uniform feature using the HOG descriptor. [14] trains a classification CNN by combining both local and global cues, which have been previously annotated. Similarly, [25] uses a pre-annotated 3D bounding box to generate a 2D “flat” representation. To alleviate the essential requirement of annotations, AM methods [5, 13, 28, 32] have been extensively researched in recent years. One common feature of them is to locate discriminative parts of a vehicle automatically using attention mechanisms. [13] aims to determine an affine transformation to map a entire vehicle to its most discriminative viewpoint in a global way. [5, 28, 32] generate features locally without using a projective transformation, and then uses them for recognition.

In contrast to previous methods, we take a further step towards taking full advantages of both the 2D and 3D representation of a vehicle. Comparing with PA and AM methods, our method is able to predict the 2D and 3D bounding box simultaneously. It can generate viewpoint normalization features using appropriate geometric constraints in a geometrically explainable way. To our best knowledge, our work is the first one to use a 3D bounding box for feature representation, which enhances recognition performance. Moreover, compared to 3D-aware methods, our method is totally free from 3D CAD models, which are difficult to obtain in practice.

Cuboid Detection: It has been observed that vertex localization typically aids cuboid detection. [7, 12, 18, 29] localize vertices using corner detectors and then construct cuboids through the geometric relationships among all vertices. Following on from the success of these geometry-based methods, [4] regresses vertices of the cuboids through a Faster-RCNN-based model. Subsequently, vertex predictions are refined by utilizing vanishing points [8]. However, this refinement step is separate from the network training stage, and the vanishing points computed from inaccurate predictions often lead to significant error. Unlike [4], we use the proposed vanishing point (VP) regularization to encode the VP constraint of the eight vertices during network training. It allows our model to avoid any post refinement to redress vertices.

ROI Pooling: ROI pooling layers, such as ROIAlign [10] and ROIWarp [3], have been extensively used in extracting fixed-size features from a rectangular ROI. However, applying them to a quadrilateral ROI is problematic. For example, extract-

ing features from the 2D bounding box of a quadrilateral RoI results in unrelated regions being included in the representation due to the irregular shape. This situation often happens when projecting rectangular regions to the image plane using a perspective transformation. To address this issue, we propose RoI Perspective (RoIPers) pooling to efficiently and effectively extract fixed-size features from quadrilateral regions caused by perspective warping. One of the key contributions is that RoIPers learns to sample corresponding feature points from the source to target through a perspective transformation.

3. Methodology

Overview: Our goal is to design an architecture that jointly extracts features in terms of both the 2D and 3D representation for vehicle recognition. The proposed model (see Figure 2) is composed of three sub-modules:

1. *Global Network*, which is a learned 2D detection network, and aims to produce global feature maps representing 2D texture information, and localize regions of interest (RoIs) that contain vehicles.
2. *3D Perspective Network*, which contains two task-specific components, 3D bounding box regression and 3D perspective feature extraction, which is obtained using the RoIPerspective layer to normalize the vehicle viewpoint in feature space.
3. *Feature Fusion Network*, which combines 2D global and 3D perspective features using multimodal compact bilinear pooling (MCB) [6], and then outputs the category of the detected vehicle.

3.1. Global Network (GN)

The GN uses a variant of RetinaNet [20] to localize the vehicle using a 2D bounding box. RetinaNet is a dense object detector composed of a CNN-FPN [19] backbone, which aims to extract a convolutional feature map, \mathcal{F}_G , over an entire input image. Two task-specific subnetworks are attached to the backbone network to perform object classification and 2D object box regression respectively. RetinaNet offers comparable performance to complex two-stage detectors [10, 23] while retaining the advantages of one-stage detectors such as inference speed and model optimization. These attributes are desirable when adopting it as one component in an end-to-end classification framework. To adapt the original RetinaNet as the part of our network, we make the following modifications:

ROIAlign process: We add an ROIAlign layer [10] after the 2D box decoding process. The detected 2D bounding box of the vehicle is denoted $B = (B_x, B_y, B_w, B_h)$, where B_x, B_y are the left-top corner coordinates with respect to x and y axis. B_w, B_h represents the width and height of B respectively. The ROIAlign layer combined with the detected 2D bounding box coordinates is able to produce a

fixed-sized global feature representation which comprises the vehicle, termed \mathcal{F}_G^B . In particular, this modification ensures that errors in the extracted 2D coordinates can be back propagated through the GN when trained jointly with other network components.

3.2. 3D Perspective Network (3DPN)

Figure 2 illustrates the architecture of the 3DPN. Its role is to provide geometrically-interpretable features by normalizing the vehicle viewpoint to account for perspective distortion. To achieve this, the 3DPN takes as input \mathcal{F}_A^B , which is the feature map pooled from B at \mathcal{F}_A using ROIAlign. \mathcal{F}_A is the auxiliary feature map extracted from an off-the-shelf CNN. We then estimate the coordinates of eight vertices of the 3D bounding box, $C : \{c^i\}_{i=0}^7$, using a 3D bounding box regression network. Subsequently, C is used to normalize the viewpoint of the vehicle in \mathcal{F}_A^B using our proposed **RoI Perspective (RoIPers)** layer. As a result, \mathcal{F}_R , \mathcal{F}_F , and \mathcal{F}_S , representing perspective transformed feature maps from the quadrilaterals formed by the roof (**R**), front (**F**), and side (**S**) of the vehicle, are extracted. Below we describe the 3D bounding box regression network with the proposed vanishing point loss, and RoIPers respectively.

3D bounding box regression branch: Instead of using the absolute coordinates of the 3D box in the image space directly, we estimate them in an RoI relative coordinate system by leveraging the 2D bounding box as an anchor. For each $\{c^i\}_{i=0}^7$ in the image coordinate system we first transform those points to the 2D-bounding-box relative coordinate system: $\hat{c}_x^i = (c_x^i - B_x - B_w/2)/B_w$, and $\hat{c}_y^i = (c_y^i - B_y - B_h/2)/B_h$, where $\{\hat{c}^i\}_{i=0}^7$ is the training target of this branch. The 3D bounding box regression network takes \mathcal{F}_A^B as the input feature map. Then it applies two conv layers ($3 \times 3 \times 256$) and a multilayer perceptron (512×16) to regress all x and y coordinates of $\{\hat{c}^i\}_{i=0}^7$ (leaky ReLu are used as activations). The loss function used to train this sub-network is:

$$L_{3D\text{branch}} = L_{\text{smooth}l_1}(\hat{c}^*, \hat{c}) + L_{\text{vp}}, \quad (1)$$

where \hat{c}^* is the ground-truth locations for \hat{c} , $L_{\text{smooth}l_1}$ is the standard smooth- l_1 loss and L_{vp} is the proposed vanishing point regularization loss to ensure that C satisfies perspective geometry (i.e., every parallel edge of C intersects at the same vanishing point).

Vanishing point regularization: A standard smooth- l_1 loss lacks the capacity to impose perspective geometry constraints on $\{c^i\}_{i=0}^7$, which constructs a projective cuboid in the image plane. We thus propose a 3D geometric vanishing point regularization loss, which forces $\{c^i\}_{i=0}^7$ to satisfy perspective geometry during regression, as such the predicted vertices don't require camera calibration data or post preprocessing for refinement [4].

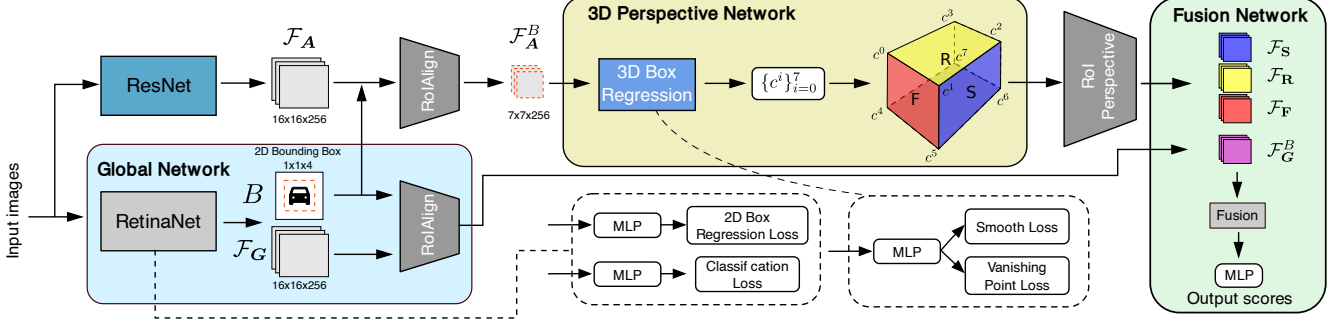


Figure 2: Overview of the proposed model. The model is composed of three main components: (A) Global Network (GN), which aims to localize the vehicle and extract its 2D features. (B) 3D Perspective Network (3DPN), which performs 3D bounding box regression by taking the anchor from the predicted 2D bounding box and generates normalized viewpoint features of the three main faces (front, roof, and side) of the vehicles. (C) Feature Fusion Network, which fuses the features from the GN and 3DPN by applying multi-modal compact bilinear (MCB) [6] pooling. **F**, **R**, **S** in the predicted 3D bounding box represents the front/rear, roof, and side respectively.

In projective geometry, the two-dimensional perspective projections of mutually parallel lines in three-dimensional space appear to converge at the vanishing point. The required condition for convergence of three lines is that the determinant of the coefficient matrix is zero. The proposed vanishing point loss encodes this geometry constraint (as shown in Figure 3) by minimizing the determinants of all sets of three parallel edges of the vehicle. Formally, taking three parallel lines $\mathbf{l}_{c^0 c^3}$, $\mathbf{l}_{c^1 c^2}$, $\mathbf{l}_{c^5 c^6}$ in **F** as examples (as shown in Figure 3), the vanishing point loss and the coefficient matrix are expressed as:

$$L_{vp_{F_1}} = (D_{vp_{F_1}})^2, D_{vp_{F_1}} = \begin{vmatrix} m_{c^0 c^3} & n_{c^0 c^3} & l_{c^0 c^3} \\ m_{c^1 c^2} & n_{c^1 c^2} & l_{c^1 c^2} \\ m_{c^5 c^6} & n_{c^5 c^6} & l_{c^5 c^6} \end{vmatrix}, \quad (2)$$

where $m_{c^i c^j}x + n_{c^i c^j}y + l_{c^i c^j} = 0$ is the line equation of $\mathbf{l}_{c^i c^j}$, and D is the determinant of the matrix. $L_{vp_{F_1}}$ is the first part of L_{vp_F} using the first three lines ($\mathbf{l}_{c^0 c^3}$, $\mathbf{l}_{c^1 c^2}$, and $\mathbf{l}_{c^5 c^6}$; see Figure 3 for details.). Similarly, we build the second part, $L_{vp_{F_2}}$, using the last three lines ($\mathbf{l}_{c^0 c^3}$, $\mathbf{l}_{c^4 c^7}$, and $\mathbf{l}_{c^5 c^6}$) in the diagonal to form up the final vanishing point regularization $L_{vp_F} = L_{vp_{F_1}} + L_{vp_{F_2}}$ for the **F** direction, and repeat for the **R** and **S** directions. Therefore, the vanishing point loss of the whole vehicle, $L_{vp} = L_{vp_R} + L_{vp_S} + L_{vp_F}$.

RoIPerspective: We propose RoIPerspective (RoIPers) pooling to ensure that when extracting features from arbitrary quadrilateral images, we sample uniformly within the quadrilateral and do not sample from points outside of it. RoIPers consists of two steps: parameterized sampling grid generation, and differentiable feature sampling. Suppose that we have a source feature map $\mathcal{F}_{\text{source}}$, which is extracted from the input image using a standard CNN, and a corresponding quadrilateral ROI, Q . The objective of RoIPers is to map the feature inside Q of $\mathcal{F}_{\text{source}}$ to a fixed-size target

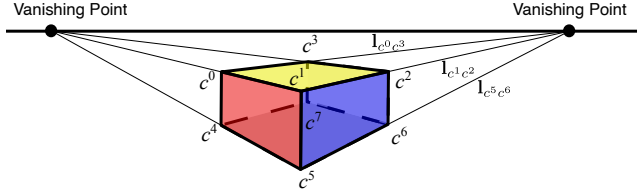


Figure 3: Illustration of the vanishing point. To simplify the visualization, only two vanishing points (in the **F** and **S** directions) are plotted. The lines $\mathbf{l}_{c^0 c^3}$, $\mathbf{l}_{c^1 c^2}$, and $\mathbf{l}_{c^5 c^6}$ contribute to the first part of L_{vp_F} .

feature map, $\mathcal{F}_{\text{target}}$. We first use a four-correspondence DLT [8] to obtain the homography \mathbf{H} between Q and $\mathcal{F}_{\text{target}}$:

$$\begin{bmatrix} q_x^i \\ q_y^i \\ 1 \end{bmatrix} \sim \begin{bmatrix} \mathbf{H}_{11} & \mathbf{H}_{12} & \mathbf{H}_{13} \\ \mathbf{H}_{21} & \mathbf{H}_{22} & \mathbf{H}_{23} \\ \mathbf{H}_{31} & \mathbf{H}_{32} & 1 \end{bmatrix} \begin{bmatrix} t_x^i \\ t_y^i \\ 1 \end{bmatrix}, \quad (3)$$

where $\{t^i\}_{i=1}^4$ and $\{q^i\}_{i=1}^4$ are the four corners of $\mathcal{F}_{\text{target}}$ and Q respectively. Thus given the coordinate of each pixel in $\mathcal{F}_{\text{target}}$, we can obtain their corresponding sampling point in $\mathcal{F}_{\text{source}}$ using \mathbf{H} . In the feature sampling step, the exact value of each sampling point at $\mathcal{F}_{\text{source}}$ can be computed easily using bilinear interpolation at four regularly sampled locations, i.e.,

$$\mathcal{F}_T^k = \sum_n \sum_m \mathcal{F}_S^{mn} \max(0, 1 - |s_x^k - m|) \max(0, 1 - |s_y^k - n|), \quad (4)$$

where k is the pixel index of $\mathcal{F}_{\text{target}}$, and s^k is the corresponding sampling point in $\mathcal{F}_{\text{source}}$. H and W are the height and width of $\mathcal{F}_{\text{target}}$ respectively. Using this approach, the feature inside Q is extracted as a fixed-size target feature map $\mathcal{F}_{\text{target}}$. Figure 4 visualizes the process of generating 3D features from \mathcal{F}_S . \mathcal{F}_R and \mathcal{F}_F can be obtained in a similar manner.

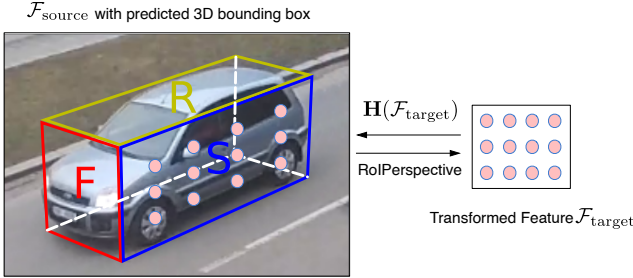


Figure 4: The process of extracting perspective corrected features from \mathbf{S} using RoIPers. $\mathcal{F}_{\text{source}}$ and $\mathcal{F}_{\text{target}}$ are the source and target feature maps respectively. To improve visualization, we show the input image overlaid with $\mathcal{F}_{\mathbf{S}}$ to show where the predicted 3D bounding box and sampling points (colored by pink) are. The sampling points in \mathbf{S} are generated using \mathbf{H} by projecting every pixel in $\mathcal{F}_{\text{target}}$ back to $\mathcal{F}_{\text{source}}$. Then the exact value of each point is computed via bilinear interpolation at four regularly sampled locations. Finally, these points are gathered to generate $\mathcal{F}_{\text{target}}$.

3.3. Feature Fusion Network (FFN)

Figure 5 visualizes the architecture of the FFN, which is designed to merge feature maps extracted from the GN and 3DPN to recognize a given vehicle. Three 3D feature representations $\mathcal{F}_{\mathbf{S}}$, $\mathcal{F}_{\mathbf{R}}$, $\mathcal{F}_{\mathbf{F}}$ and one global feature $\mathcal{F}_{\mathbf{G}}^B$ are processed through two identity blocks [11], followed by a global average pooling (GAP) layer, to generate refined feature vectors respectively. Please note that the three feature vectors from \mathbf{F} , \mathbf{R} , and \mathbf{S} are concatenated together to form a single perspective feature vector carrying discriminative perspective information representing different vehicle views. The final feature vector, whose size is 16000, is obtained by applying multi-modal compact bilinear (MCB) [6] pooling on the global and perspective feature vector. The reason for using MCB is that it is normally used to facilitate the joint optimization of two networks generating features which lie on different manifolds. The two feature vectors are obtained from two different networks (GN vs. 3DPN), i.e., they lie on different manifolds. The final feature vector is passed through two fully-connected (fc) layers of size 2048 and the number of categories, respectively. Up to this point, our full model, which is composed of three network components, can be trained jointly with a single optimization process using the following multi-task loss function:

$$L = \lambda_1 L_{2\text{DGN}} + \lambda_2 L_{3\text{DPN}} + \lambda_3 L_{\text{CrossEntropy}}, \quad (5)$$

where $L_{2\text{DGN}}$ is the focal loss [20] used to train the GN, $L_{3\text{DPN}}$ is defined in Equation 1, and $L_{\text{CrossEntropy}}$ is the cross entropy loss to train the last softmax layer in the FFN.

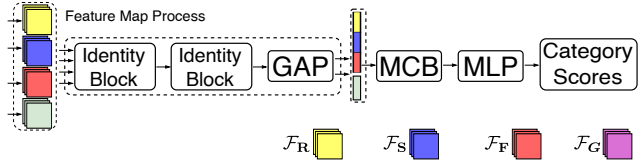


Figure 5: Feature Fusion Network (FFN) architecture. Four feature maps are processed by two identity blocks and global average pooling (GAP) to generate corresponding feature vectors. Then these feature vectors are merged using multi-modal compact bilinear (MCB) pooling, followed by two fully-connected layers, to output the final category scores.

4. Experiments

To our best knowledge, the BoxCars dataset [25] is only dataset which provides both 3D and 2D bounding box annotations for vehicle recognition in the computer vision community. Therefore, we use it to evaluate our model. BoxCars contains 63,750 images, which are collected from 21,250 vehicles of 27 different makes. All images are taken from surveillance cameras. BoxCars consists of two challenging tasks: classification and verification. Regarding the classification task, the dataset is split into two subsets: *Medium* and *Hard*. The *Hard* protocol has 87 categories and contains 37,689 training images and 18,939 testing images. The *Medium* protocol is composed of 77 categories and has 40,152 and 19,590 images for training and testing respectively. The main difference between the *Medium* and *Hard* splits is that *Hard* considers make, model, submodel, and model year; while *Medium* does not differentiate model year. With respect to the verification task, BoxCars has three well defined protocols that provide *Easy*, *Medium*, and *Hard* cases. The *Easy* protocol is composed of pairs of vehicle images recorded from the same unseen camera. Camera identities are no longer fixed in the *Medium* protocol. The *Hard* protocol not only draws vehicle pairs from different unseen cameras, but also takes into account vehicle model years.

4.1. Implementation Details

GN and 3DPN Architecture: The RetinaNet [20] backbone used in the GN is built on MobileNetV2 [24]. ResNet101 [11] with the first 4 stages is selected as the 3DPN architecture. We select different backbones for 3DPN and GN because features produced from them lie on different manifolds. This can enhance the representation of the unified network.

Training and Optimization: We have implemented our model using Keras [2] and TensorFlow [1]. In this paper, we adopt a pragmatic 2-step training approach to optimize the whole network. In the first step, we train the GN solely so that it can output the 2D bounding box correctly, which is important to train the 3DPN which takes the 2D bounding box as input. In

the second step, we train all three network components, the GN, 3DPN, and FFN, together in an end-to-end manner. λ_1 , λ_2 , λ_3 are set to 1, 0.1, and 1 respectively. SGD is chosen as our optimizer and its momentum is set to 0.9. The initial learning rate is 0.02, and is divided by 10 after every 15 epochs. The batch size is set to 30. The model optimisation is ceases when training reaches 45 epochs. Each batch takes approximately 2s on a NVIDIA Tesla P100 GPU and in total the model takes about 12 hours to converge.

4.2. Vehicle Classification Results

Baselines: Since our model recognize vehicles from a single image, only state-of-the-art methods [11, 17, 20, 23–25] which use a single image are selected to compare with our method. These methods are divided into two evaluation categories: (1) detection-like (*det*-like) networks [20, 23], in which localization and classification of the vehicle are performed simultaneously; and (2) classification-like (*cls*-like) networks [5, 13, 25, 28, 32] in which vehicles are cropped using annotated bounding box before network training. Since our model is composed of a RetinaNet built by MobileNetV2, detection-like networks [20, 23] also built with MobileNetV2 are compared to ours to demonstrate that the performance gain is due to the use of the 3D feature representation. Regarding attention mechanism methods, [5, 13, 25, 28, 32] are used to demonstrate the efficiency of our method that uses both the 2D and 3D feature representation. We note that [25] superficially resembles our method. However, [25] requires 3D bounding box annotations to preprocess images before network training, and the vehicle in the image is still “flat”, i.e., lacking of 3D meaning. Furthermore, [25] requires annotated 3D boxes at inference time, while the proposed approach operate over the raw image with no further input. With respect to classification-like networks, all images are resized to 224×224 . Regarding detection-like networks, images are resized to the same scale of 256 pixels as in [19]. To make fair comparison, we use the official implementations of these methods without any parameter changes.

***det*-like network results:** The upper half of Table 1 shows the results of *det*-like networks. One can see that Ours-*det* surpasses all *det*-like baselines by a significant margin. Since RetinaNet [20] and Faster-RCNN [23] shares the same backbone (MobileNetV2) with the GN in Ours-*det*, we confirm that the additional 3D feature representation significantly improves the performance obtained compared to using traditional 2D features. From Table 1, one can see that RetinaNet and Faster-RCNN do not have a top-5 accuracy recorded. This is because RetinaNet and Faster-RCNN output confidence scores of predicted boxes. After non-maximum suppression, the boxes with high confidence scores are merged, and as such there is only a top-1 accuracy. Although non-maximum suppression is also performed in our method, we can still obtain top-5 accuracy due to the use of the softmax layer in the FFN.

***cls*-like network results:** To make a comparison between *cls*-like baselines and the proposed approach, we modify the 2D processing component of our model. Specifically, MobileNetV2-based RetinaNet is replaced with a vanilla MobileNetV2, in which the last global average pooling layer and following classification layer are removed. Therefore the output of this network is used as a global feature for the vehicle. The modified model for *cls*-like experiments is denoted Ours-*cls*.

The second half of Table 1 showcases overall classification accuracy (percent) for *cls*-like networks. We observe that Ours-*cls* consistently performs better than all baseline models with respect to classification accuracy in both the *Medium* and *Hard* splits. One can see that [5, 13] perform poorly among all *cls*-like methods, as [5, 13] only search for the most discriminative part of a vehicle. This strategy discards parts of the global feature, which captures important pose information and other subtle details. Moreover, an affine transformation used in [13] significantly increases the difficulty of vehicle viewpoint normalization. This is because an affine transformation of the 2D vehicle bounding box distorts the shape of the vehicle, and does not consider its 3D geometry. We next compare Ours-*cls* with previous state-of-the-art methods [25, 28, 32], which extract discriminative features without considering the 3D geometry. From the results, we conjecture that the combined 2D and 3D representation used in our method has better a capability for distinguishing vehicle details than other methods. Last but not least, Ours-*cls* is the only method which can extract the 3D structure of a vehicle. In contrast to [5, 13, 25, 28, 32], Ours-*cls* normalizes the viewpoint of a car in a geometrically correctly way, i.e., performing a perspective transformation on each side of the predicted 3D bounding box. This 3D-bounding-box based feature representation retains pose information as well as discriminative texture details from each face, and as such the feature representation has good generality.

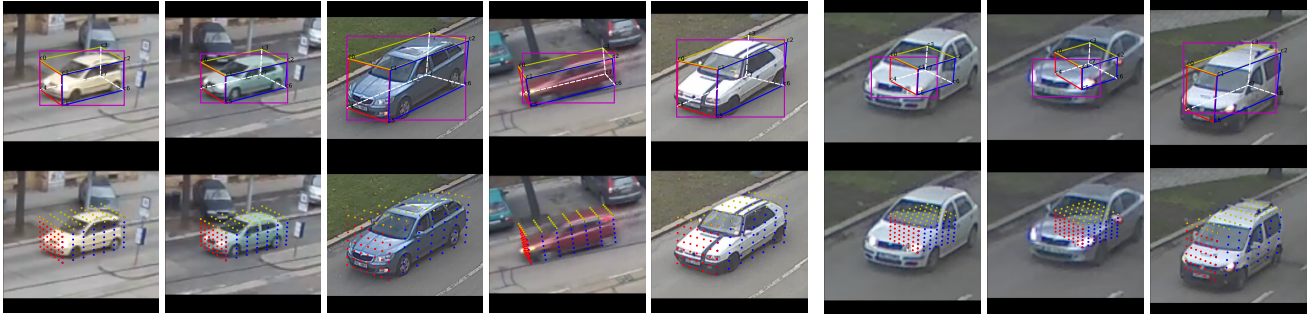
Qualitative results: Figure 6 visualizes qualitative results on BoxCars images. In Figure 6 (a), we see that Ours-*det* is able to determine the correct 2D location and 3D bounding box estimation of the vehicle. Figure 6 (b) shows some mis-estimated images. The first two columns show 3D bounding box regression performance, in situations where the 2D bounding box is incorrect, and the 3D estimation cannot recover from the earlier error. The last column shows a case where 2D location is predicted correctly and the 3D box estimator fails. We see that the 3D bounding box estimation tries to compensate for errors made by the 2D bounding box estimation. In addition, the sampling points computed by RoiPers for **F**, **R**, and **S** are also shown. One can see that the sampling points perfectly cover the three main sides of the vehicles, and therefore extract perspective invariant features.

4.3. Ablation experiments

An ablation study is conducted to analyze the effectiveness of the individual proposed components including RoiPers,

Table 1: Overall classification accuracy on BoxCars dataset. M and H represent the *Medium* and *Hard* splits. Top-1 and -5 accuracy are denoted as T-1 and T-5.

Method	Input Size	Detection?	3D?	Attention?	M T-1	M T-5	H T-1	H T-5
RetinaNet [20]	256×256	✓	✗	✗	66.52	-	59.4	-
Faster-RCNN [23]	256×256	✓	✗	✗	67.23	-	62.73	-
Ours-det	256×256	✓	✓	✓	78.45	93.39	75.18	91.53
NTS [32]	224×224	✗	✗	✓	80.40	92.37	76.31	90.42
DFL [28]	224×224	✗	✗	✓	76.78	91.94	70.25	88.405
BoxCar [25]	224×224	✗	✗	✓	75.4	90.1	73.1	89
RACNN [5]	224×224	✗	✗	✓	72.21	88.47	67.5	86.83
STN [13]	224×224	✗	✗	✓	64.33	81.92	59.76	80.13
Ours-cls	224×224	✗	✓	✓	81.27	93.82	77.08	91.97



(a) The correctly predicted examples.

(b) The mispredicted examples.

Figure 6: Qualitative results visualization of Ours-det on BoxCars dataset. (a): examples in which the 2D and 3D bounding box are correctly predicted. (b): examples containing errors in prediction. The first row shows 2D and 3D bounding box estimations by our proposed method. The 2D detected bounding box is denoted using a magenta box. The 3D bounding box is colored to indicate quadrilateral regions: red is the front, blue is the side and yellow is the roof. The second row represents the corresponding sampling points computed by RoIPers (Sec. 3.2).

the VP regularization loss and network design in the 3D bounding box regression component.

RoIPers vs. RoIAlign: In this experiment we compare the performance of the proposed RoIPers to the frequently used RoIAlign on the *Hard* and *Medium* splits. The RoIPers layers in Ours-det are replaced with RoI Align to evaluate the impact of RoIPers. The results are shown in Table 2. It can be observed that network employing RoIPers instead of RoI Align achieves approximately 6.1% and 2.1% improvement on *Medium* and *Hard* splits. As discussed in Sec. 3, RoIPers can extract relevant features from arbitrary quadrilateral regions. In contrast, RoIAlign introduces unrelated information/noise using the bounding rectangles of quadrilateral RoIs, which may harm the process of extracting useful features from the unaligned vehicle images.

VP regularization: We evaluate the proposed VP regularization loss on 3D bounding box detection. The baseline we compare against is [4], where a Faster-RCNN-based model is implemented to detect cuboids. To make a fair comparison, we add VP regularization directly to [4], and as such the only difference between these two methods is the use of vanishing

Table 2: Classification accuracy results with different RoI layers in terms of the *Medium* and *Hard* splits on the BoxCars dataset.

RoI Pooling Type	M . T-1	M . T-5	H . T-1	H . T-5
RoI Align	73.97	91.23	73.65	91.13
RoI Pers.	78.45	93.39	75.18	91.53

Table 3: Evaluation of 3D bounding box localization and quality using the percentage of correct keypoints (PCK) and the proposed cuboid quality (CQ). e stands for the number of training epochs.

	e=5		e=10		e=15	
	PCK	CQ	PCK	CQ	PCK	CQ
Ours-det	85.35	1.48	85.66	1.98	87.15	2.12
DeepCuboid [4]	85.03	1.48	85.58	1.64	86.70	1.69

point regularization or not. Table 3 reports the results obtained in the *Hard* split in terms of two metrics, the percentage of correct points (PCK) [27, 31] and the proposed cube quality (CQ).

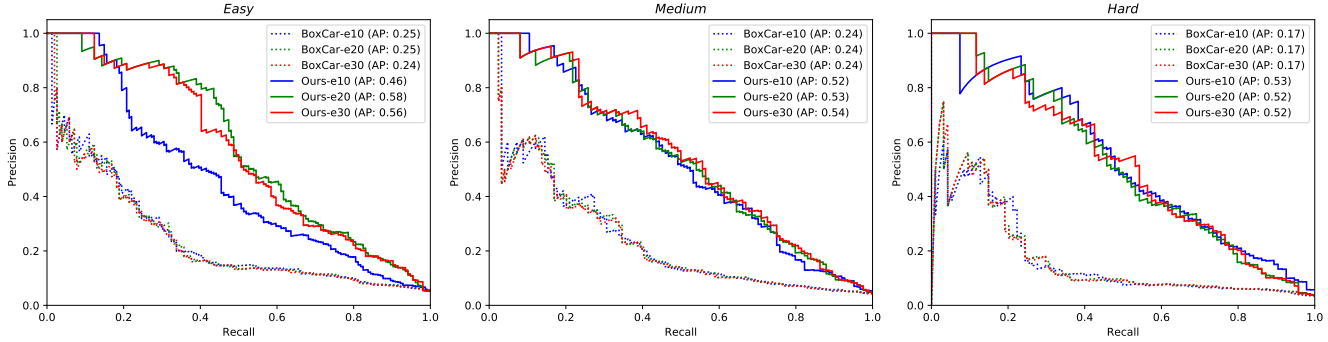


Figure 7: Precision-Recall (PR) curves of different models with different training epoch (e denotes training epoch x). Three verification protocols *Easy*, *Medium*, and *Hard* are shown in the figure. Average Precision (AP) is given in the plot legends. Baseline results (shown as BoxCar-ex) are taken from [25].

Table 4: The converged smooth- l_1 loss obtained from different designs of the 3D bounding box regression branch. Fully convolutional networks (FCN) and multi-layer perceptrons (MLP) architectures are compared.

	3D Bounding Box Regression Branch	loss
FCN	conv: 256 \rightarrow 256 \rightarrow 512	0.018
MLP	fc: 256 \rightarrow 256 \rightarrow 512	0.016
MLP	fc: 256 \rightarrow 256 \rightarrow 512 \rightarrow 512	0.015

A predicted vertex is considered to be correct if it lies within $0.1 \times (\max(\text{height}, \text{width}))$ pixels of the ground truth annotation of the vertex. CQ is computed via $-\log L_{\text{VP}}$, where L_{VP} is the loss defined in Sec. 3.2. From the results, we can see that the 3D bounding box obtained from our method with VP regularization consistently outperforms that of [4] in terms of both metrics. In the early and mid training stages (the fifth and tenth epochs), our method is equal or slightly better than [4]. However, as the model is trained with more epochs, our method surpasses [4] by a larger margin in terms of both the PCK and CQs; demonstrating that the proposed vanishing point regularization is of benefit to the 3D cuboid prediction in both quality and accuracy.

3D bounding box regression branch: Here we explore architectures of the sub-network in terms of two designs, i.e., fully convolution networks (FCN) and multi-layer perceptrons (MLP) in the 3DPN (Sec. 3.2). Table 4 reports the converged smooth- l_1 loss for test images obtained from different designs. We show that the FCNs achieve approximately the same smooth- l_1 loss as an MLP-based branch does. However, the number of parameters in the MLP network is 100 times more than the FCN. Considering computational complexity and model efficiency, we employ an FCN to perform the 3D bounding box regression.

4.4. Vehicle Verification

Vehicle verification is the problem of determining whether two gallery samples belong to the same category. It is an important

and challenging task for intelligence transportation, especially when the system is working under new scenarios with unseen and misaligned categories.

To demonstrate the generality and robustness of the proposed method, we conduct experiments on the verification task of BoxCars. In this experiment, we follow the same method of [25] to perform verification, i.e., 3,000 image pairs are randomly selected to test the performance of various models in each case.

For all networks, we use the output of the second last layer (the layer preceding the last softmax classification layer) as the representation feature vector for the given image. For each image pair, we use the cosine distance [26] to obtain the similarity of two gallery images, which is then used to compute precision, recall, and average precision.

The precision-recall (PR) curves presented in Figure 7 show that the proposed approach outperforms the baseline method [25] on all three dataset protocols. The performance gain of our method provides an absolute performance gain of 33% in Average Precision (AP) on *Easy*, and an even better 36% AP on the *Hard* split. It is worth noting that the size of feature vector of [25] is 4096 while ours is 2048, which indicates a better data distribution and faster speed for model inference.

5. Conclusions

In this paper, we propose a unified framework to perform fine-grained vehicle classification, which takes full advantage of both the 2D and 3D perspective representations. The proposed method achieves the state-of-the-art results both in car classification and verification in the BoxCars dataset. Furthermore, we propose vanishing point regularization for cuboid detection, which is intuitively appealing and geometrically explainable, and avoids the need for a post detection refinement processes, as used by existing methods. Last but not least, the proposed ROI Perspective is able to extract features from ROIs warped by perspective efficiently; and is able to extract features that are more effective than existing the state-of-the-art method [10].

References

[1] M. Abadi, P. Barham, J. Chen, Z. Chen, A. Davis, J. Dean, M. Devin, S. Ghemawat, G. Irving, M. Isard, et al. Tensorflow: a system for large-scale machine learning. In *OSDI*, volume 16, pages 265–283, 2016.

[2] F. Chollet et al. Keras, 2015.

[3] J. Dai, K. He, and J. Sun. Instance-aware semantic segmentation via multi-task network cascades. In *Proceedings of the IEEE Conference on Computer Vision and Pattern Recognition*, pages 3150–3158, 2016.

[4] D. Dwibedi, T. Malisiewicz, V. Badrinarayanan, and A. Rabenovich. Deep cuboid detection: Beyond 2d bounding boxes. *arXiv preprint arXiv:1611.10010*, 2016.

[5] J. Fu, H. Zheng, and T. Mei. Look closer to see better: Recurrent attention convolutional neural network for fine-grained image recognition. In *Proceedings of the IEEE conference on computer vision and pattern recognition*, pages 4438–4446, 2017.

[6] A. Fukui, D. H. Park, D. Yang, A. Rohrbach, T. Darrell, and M. Rohrbach. Multimodal compact bilinear pooling for visual question answering and visual grounding. *arXiv preprint arXiv:1606.01847*, 2016.

[7] A. Gupta, S. Satkin, A. A. Efros, and M. Hebert. From 3d scene geometry to human workspace. In *Computer Vision and Pattern Recognition (CVPR), 2011 IEEE Conference on*, pages 1961–1968. IEEE, 2011.

[8] R. Hartley and A. Zisserman. *Multiple view geometry in computer vision*. Cambridge university press, 2003.

[9] H. He, Z. Shao, and J. Tan. Recognition of car makes and models from a single traffic-camera image. *IEEE Transactions on Intelligent Transportation Systems*, 16(6):3182–3192, 2015.

[10] K. He, G. Gkioxari, P. Dollár, and R. Girshick. Mask r-cnn. In *Computer Vision (ICCV), 2017 IEEE International Conference on*, pages 2980–2988. IEEE, 2017.

[11] K. He, X. Zhang, S. Ren, and J. Sun. Deep residual learning for image recognition. In *Proceedings of the IEEE conference on computer vision and pattern recognition*, pages 770–778, 2016.

[12] V. Hedau, D. Hoiem, and D. Forsyth. Recovering free space of indoor scenes from a single image. In *2012 IEEE Conference on Computer Vision and Pattern Recognition*, pages 2807–2814. IEEE, 2012.

[13] M. Jaderberg, K. Simonyan, A. Zisserman, et al. Spatial transformer networks. In *Advances in neural information processing systems*, pages 2017–2025, 2015.

[14] J. Krause, T. Gebru, J. Deng, L. Li, and L. Fei-Fei. Learning features and parts for fine-grained recognition. In *2014 22nd International Conference on Pattern Recognition*, pages 26–33, Aug 2014.

[15] J. Krause, H. Jin, J. Yang, and L. Fei-Fei. Fine-grained recognition without part annotations. In *Proceedings of the IEEE Conference on Computer Vision and Pattern Recognition*, pages 5546–5555, 2015.

[16] J. Krause, M. Stark, J. Deng, and L. Fei-Fei. 3d object representations for fine-grained categorization. In *Proceedings of the IEEE International Conference on Computer Vision Workshops*, pages 554–561, 2013.

[17] A. Krizhevsky, I. Sutskever, and G. E. Hinton. Imagenet classification with deep convolutional neural networks. In *Advances in neural information processing systems*, pages 1097–1105, 2012.

[18] D. C. Lee, M. Hebert, and T. Kanade. Geometric reasoning for single image structure recovery. In *Computer Vision and Pattern Recognition, 2009. CVPR 2009. IEEE Conference on*, pages 2136–2143. IEEE, 2009.

[19] T.-Y. Lin, P. Dollár, R. B. Girshick, K. He, B. Hariharan, and S. J. Belongie. Feature pyramid networks for object detection. In *CVPR*, volume 1, page 4, 2017.

[20] T.-Y. Lin, P. Goyal, R. Girshick, K. He, and P. Dollár. Focal loss for dense object detection. *IEEE transactions on pattern analysis and machine intelligence*, 2018.

[21] Y.-L. Lin, V. I. Morariu, W. Hsu, and L. S. Davis. Jointly optimizing 3d model fitting and fine-grained classification. In *European Conference on Computer Vision*, pages 466–480. Springer, 2014.

[22] Y. Peng, X. He, and J. Zhao. Object-part attention model for fine-grained image classification. *IEEE Transactions on Image Processing*, 27(3):1487–1500, 2018.

[23] S. Ren, K. He, R. Girshick, and J. Sun. Faster r-cnn: Towards real-time object detection with region proposal networks. In *Advances in neural information processing systems*, pages 91–99, 2015.

[24] M. Sandler, A. Howard, M. Zhu, A. Zhmoginov, and L.-C. Chen. Mobilenetv2: Inverted residuals and linear bottlenecks. In *Proceedings of the IEEE Conference on Computer Vision and Pattern Recognition*, pages 4510–4520, 2018.

[25] J. Sochor, A. Herout, and J. Havel. Boxcars: 3d boxes as cnn input for improved fine-grained vehicle recognition. In *2016 IEEE Conference on Computer Vision and Pattern Recognition (CVPR)*, pages 3006–3015, June 2016.

[26] Y. Taigman, M. Yang, M. Ranzato, and L. Wolf. Deepface: Closing the gap to human-level performance in face verification. In *Proceedings of the IEEE conference on computer vision and pattern recognition*, pages 1701–1708, 2014.

[27] S. Tulsiani and J. Malik. Viewpoints and keypoints. In *Proceedings of the IEEE Conference on Computer Vision and Pattern Recognition*, pages 1510–1519, 2015.

[28] Y. Wang, V. I. Morariu, and L. S. Davis. Learning a discriminative filter bank within a cnn for fine-grained recognition. In *Proceedings of the IEEE Conference on Computer Vision and Pattern Recognition*, pages 4148–4157, 2018.

[29] M. Wilczkowiak, P. Sturm, and E. Boyer. Using geometric constraints through parallelepipeds for calibration and 3d modeling. *IEEE transactions on pattern analysis and machine intelligence*, 27(2):194–207, 2005.

[30] T. Xiao, Y. Xu, K. Yang, J. Zhang, Y. Peng, and Z. Zhang. The application of two-level attention models in deep convolutional neural network for fine-grained image classification. In *Proceedings of the IEEE Conference on Computer Vision and Pattern Recognition*, pages 842–850, 2015.

[31] Y. Yang and D. Ramanan. Articulated human detection with flexible mixtures of parts. *IEEE transactions on pattern analysis and machine intelligence*, 35(12):2878–2890, 2013.

- [32] Z. Yang, T. Luo, D. Wang, Z. Hu, J. Gao, and L. Wang. Learning to navigate for fine-grained classification. In *Proceedings of the European Conference on Computer Vision (ECCV)*, pages 420–435, 2018.
- [33] H. Zheng, J. Fu, T. Mei, and J. Luo. Learning multi-attention convolutional neural network for fine-grained image recognition. In *Int. Conf. on Computer Vision*, volume 6, 2017.